Discrete dislocation plasticity analysis of crack-tip fields in polycrystalline materials

Balint, DS; Deshpande, VS; Needleman, A; Van Der Giessen, E

Published in:
Philosophical Magazine

DOI:
10.1080/14786430500073887

Philosophical Magazine,
Vol. 85, Nos. 26–27, 11–21 September 2005, 3047–3071

Taylor & Francis
Taylor & Francis Group

Discrete dislocation plasticity analysis of crack-tip fields in polycrystalline materials

D. S. BALINT†, V. S. DESHPANDE†, A. NEEDLEMAN*‡ and E. VAN DER GIESSEN§

†Cambridge University, Department of Engineering, Trumpington Street, Cambridge CB2 1PZ, UK
‡Brown University, Division of Engineering, Providence, RI 02912, USA
§University of Groningen, Department of Applied Physics, Nyenborgh 4, 9747 AG Groningen, The Netherlands

(*Received 12 November 2004; in final form 17 January 2005*)

Small scale yielding around a mode I crack is analysed using polycrystalline discrete dislocation plasticity. Plane strain analyses are carried out with the dislocations all of edge character and modelled as line singularities in a linear elastic material. The lattice resistance to dislocation motion, nucleation, interaction with obstacles and annihilation are incorporated through a set of constitutive rules. Grain boundaries are modelled as impenetrable to dislocations. The polycrystalline material is taken to consist of two types of square grains, one of which has a bcc-like orientation and the other an fcc-like orientation. For both orientations there are three active slip systems. Alternating rows, alternating columns and a checker-board-like arrangement of the grains is used to construct the polycrystalline materials. Consistent with the increasing yield strength of the polycrystalline material with decreasing grain size, the calculations predict a decrease in both the plastic zone size and the crack-tip opening displacement for a given applied mode I stress intensity factor. Furthermore, slip-band and kink-band formation is inhibited by all grain arrangements and, with decreasing grain size, the stress and strain distributions more closely resemble the HRR fields with the crack-tip opening approximately inversely proportional to the yield strength of the polycrystalline materials. The calculations predict a reduction in fracture toughness with decreasing grain size associated with the grain boundaries acting as effective barriers to dislocation motion.

1. Introduction

The plastic dissipation around a crack tip in crystalline metals results in the work of fracture being much larger than the work required to separate the crack surfaces (e.g. Irwin [1] and Tvergaard and Hutchinson [2]). Hence, plastic flow in the vicinity of a crack tip is key for determining the fracture resistance of ductile metals. Indeed, the analyses of asymptotic crack-tip fields in isotropic strain hardening solids by Hutchinson [3] and Rice and Rosengren [4] (the HRR fields), and in ideally plastic

*Corresponding author. Email: alan_needleman@brown.edu

Philosophical Magazine
ISSN 1478–6435 print/ISSN 1478–6443 online © 2005 Taylor & Francis
http://www.tandf.co.uk/journals
DOI: 10.1080/14786430500073887

single crystals by Rice [5] have provided the basis for the current understanding of the fracture behaviour of ductile metals.

The HRR fields are often appropriate to model crack-tip fields at the macroscopic scale, averaging over many grains. When the crack-tip opening is much less than the grain size, the plastic crack-tip fields are contained in a single crystal. At this scale, the discreteness of the slip systems plays a major role in setting the crack-tip fields. Using continuum slip theory, Rice [5] analysed these fields for a non-hardening crystal and subsequently Saeedvafa and Rice [6] extended the analysis to power-law hardening crystals. Typically, classical continuum plasticity analyses predict that the maximum stress attained at a blunted mode I crack tip is of the order of three to five times the material's flow strength.

Cleveringa *et al.* [7] carried out an analysis that accounts for the discreteness of dislocations in single crystals; i.e. plasticity is described in terms of the collective motion of large numbers of discrete dislocations. They found that, away from the very-near crack-tip region, the stress variation was consistent with the main features of Rice's continuum slip solution [5]. However, in the very-near crack-tip region, the opening stress magnitude was about a factor of seven higher than predicted by continuum slip plasticity. The analyses in Cleveringa *et al.* [7] showed that dislocations play a dual role. On the one hand, the dissipation associated with dislocation motion results in the toughness being much greater than that associated with the work of creating new surface. On the other hand, the local stress concentration associated with discrete dislocation patterning promotes fracture.

The mechanical properties of nano and ultra-fine grained crystalline alloys with grain sizes in the range 5 nm to 10 μm have received considerable attention over the past few years with numerous investigations of their yield and fatigue properties (see Kumar *et al.* [8] for a critical appraisal of the current state of understanding). In particular, experimental (e.g. Chokshi *et al.* [9]) and molecular dynamics studies (e.g. Van Swygenhoven *et al.* [10]) have indicated that the yield strength increases with decreasing grain size as per the Hall–Petch effect to grain sizes of about 10 nm. At smaller grain sizes the strength either remains constant or decreases. In contrast, there is little to no systematic data on the variation of fracture properties with grain size for such materials. The size (and time) scales that can currently be analysed with molecular dynamics precludes consideration of the full range of scales over which the fracture process occurs.

In this paper, we employ the discrete dislocation plasticity formulation in Van der Giessen and Needleman [11] to investigate stationary crack-tip fields and crack growth in polycrystals with grain sizes ranging from 200 nm to 5 μm. A key feature of the approach is that the material model and fracture properties are independent, with the material model applicable whether or not there is a crack. The fracture properties are embedded in a cohesive surface constitutive relation and thus crack growth, which is stress as well as deformation driven, occurs as a natural outcome of the boundary value problem solution. A plane strain small-scale yielding boundary value problem is formulated and solved with plasticity occurring due to the glide of a large number of edge dislocations on specified slip planes and grain boundaries taken to be impenetrable to dislocations. The solutions of the boundary value problem are used to investigate the transition from single crystal to polycrystal stationary crack-tip fields and to explore the effect of grain size on fracture toughness.

2. Discrete dislocation formulation for polycrystals

A quasi-static formulation is used with the crystals taken to be elastically isotropic with Young's modulus $E = 70\,\text{GPa}$ and Poisson's ratio $\nu = 0.33$. Plane strain conditions are assumed with the $x_1 - x_2$-plane the plane of deformation and geometry changes are neglected. Each square grain of side d has three slip systems (denoted by $\alpha = 1$, 2, or 3) at an angle $\phi^{(\alpha)}$ relative to the x_1-axis. The geometry and arrangement of the grains in the polycrystals analysed are described in section 2.4.

Plastic deformation, when it occurs, is described by the nucleation and glide of discrete edge dislocations, represented as line singularities in an elastic medium, with Burgers vector $b = 0.25\,\text{nm}$. Once dislocations nucleate, field quantities are computed using superposition. The singular ($\tilde{}$) field associated with the N dislocations is calculated analytically from the isotropic linear elastic fields. Both pure shear and mode I small scale yielding crack calculations are carried out. For the pure shear calculations, the infinite medium fields (e.g. Friedel [12], Hirth and Lothe [13], Nabarro [14]) of the dislocations are employed as the ($\tilde{}$) fields while for the crack calculations, dislocations fields in a half-space $x_2 \geq 0$ [15] are employed for numerical convenience. The complete solution is obtained by adding an image ($\hat{}$) field that ensures that the boundary conditions are satisfied. Thus, the displacements, strains and stresses are expressed as

$$u_i = \hat{u}_i + \tilde{u}_i, \quad \epsilon_{ij} = \hat{\epsilon}_{ij} + \tilde{\epsilon}_{ij}, \quad \sigma_{ij} = \hat{\sigma}_{ij} + \tilde{\sigma}_{ij}, \tag{1a}$$

respectively, where the ($\tilde{}$) field is the sum of the fields of the individual dislocations in their current positions, i.e.

$$\tilde{u}_i = \sum_{I=1}^{N} \tilde{u}_i^{(I)}, \quad \tilde{\sigma}_{ij} = \sum_{I=1}^{N} \tilde{\sigma}_{ij}^{(I)}, \quad \tilde{\epsilon}_{ij} = \sum_{I=1}^{N} \tilde{\epsilon}_{ij}^{(I)}. \tag{1b}$$

The image ($\hat{}$) field is obtained by solving a linear elastic boundary value problem with boundary conditions that change as the dislocation structure evolves [11].

2.1. *Dislocation dynamics*

At the beginning of a calculation the polycrystal is stress- and dislocation-free. Dislocation sources, which mimic Frank–Read sources, are randomly distributed on slip planes spaced $100b$ apart, with a density $\rho_{\text{nuc}} = 20\,\mu\text{m}^{-2}$ in all grains. Each source is randomly assigned a nucleation strength, τ_{nuc}, from a Gaussian distribution with average $\bar{\tau}_{\text{nuc}} = 46\,\text{MPa}$ and standard deviation 9.2 MPa. A dislocation dipole is nucleated when the resolved shear stress at a source is greater than the nucleation strength τ_{nuc} for the nucleation time $t_{\text{nuc}} = 10\,\text{ns}$. The sign of the dipole is determined by the sign of the resolved shear stress. The distance between the two dislocations at nucleation, L_{nuc}, is taken such that the attractive stress field that the dislocations exert on each other is equilibrated by a shear stress of magnitude τ_{nuc}.

After nucleation, the dislocations glide apart, driven by the Peach–Koehler force acting on them. The Peach–Koehler force on dislocation I is calculated as

$$f^{(I)} = n_i^{(I)} \left[\hat{\sigma}_{ij} + \sum_{J \neq I} \tilde{\sigma}_{ij}^{(J)} + S_{ij}^{(I)} \right] b_j^{(I)}, \tag{2}$$

where $n_i^{(I)}$ is the unit normal to the slip system on which dislocation I with Burgers vector $b_j^{(I)}$ resides and $S_{ij}^{(I)}$ are the non-singular components of $\tilde{\sigma}_{ij}^{(I)}$. Dislocation glide is taken to be drag controlled, with zero Peierls stress, so that the velocity of dislocation I is computed directly from the Peach–Koehler force as $v^{(I)} = f^{(I)}/B$, where the drag coefficient is $B = 10^{-4}$ Pa s. Obstacles are randomly distributed with a density $\rho_{\text{obs}} = 40\,\mu\text{m}^{-2}$ in all grains. Dislocations that encounter obstacles are pinned. Obstacles release pinned dislocations when the Peach–Koehler force exceeds $\tau_{\text{obs}} = 150$ MPa. When two dislocations of opposite sign are not farther apart than the annihilation distance, $6b$, they are removed. The grain boundaries are taken to be impenetrable to dislocations.

2.2. *Pure shear calculations*

In order to determine the response of the polycrystals to an overall homogeneous deformation state, the pure shear boundary value problem sketched in figure 1a is analysed. The polycrystal consists of a doubly periodic array of square unit cells of side $L = kd$, where d is the grain size and k the number of grains along a side of the unit cell. The unit cell is subject to pure shear, prescribed through the displacement boundary condition

$$\Delta u_i = \bar{\epsilon}_{ij} \, \Delta x_j, \tag{3}$$

where Δu_i is the difference between displacements on opposite sides of the unit cell specified by the difference position vector Δx_j. The strain components are specified as $\bar{\epsilon}_{12} = \bar{\epsilon}_{21} = \gamma/2$ and $\bar{\epsilon}_{11} = \bar{\epsilon}_{22} = 0$, with γ the applied shear strain. The work-conjugate shear stress is

$$\tau = \frac{1}{2L^2} \int_C (T_1 x_2 + T_2 x_1) \, dC, \tag{4}$$

where $T_i = \sigma_{ij} n_j$ is the traction on the boundary C of the unit cell with n_j the outward unit normal.

Since the $\tilde{(\,)}$ field is constructed from the known analytical fields for dislocations in an infinite medium, the $\tilde{(\,)}$ field is aperiodic, and overall periodicity is enforced via the $\hat{(\,)}$ field such that the boundary conditions (3) are satisfied.

The doubly-periodic pure shear calculations were carried out on $L = 6\,\mu$m unit cells for grain sizes d ranging from $0.2\,\mu$m to $3.0\,\mu$m, and for an $L = 10\,\mu$m unit cell for the $d = 5.0\,\mu$m material. The shear response of a single crystal was also calculated for reference purposes. In the polycrystal calculations, all boundaries of the periodic cell coincide with grain boundaries and so are impenetrable to dislocations. On the other hand, for a single crystal, the cell boundaries do not impede dislocation motion

so that when dislocations reach the boundary of the unit cell they are re-introduced into the unit cell from the opposite boundary while retaining their slip contribution.

Resolving the dislocation dynamics requires a small time step of $\Delta t = 0.5\,\text{ns}$. Thus, the calculations were carried out with a rather high loading rate of $\dot{\gamma} = 200\,\text{s}^{-1}$ in order to reduce the CPU time required for the computations. A more complete description of the pure shear calculations is given in Balint *et al*. [16].

2.3. *Mode I crack calculations*

The plane strain small-scale yielding problem analysed is sketched in figure 1b and the boundary value problem formulation and solution procedure are outlined here. Further details and references are given in Cleveringa *et al*. [7] and Van der Giessen *et al*. [17]. The origin of the coordinate system coincides with the initial position

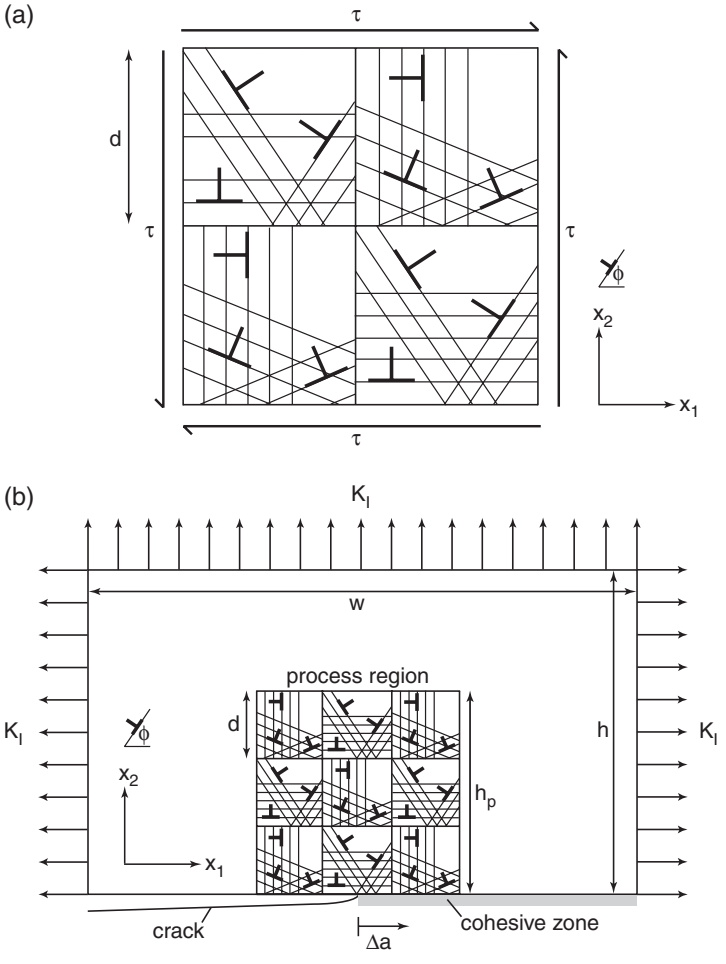

Figure 1. Sketch of (a) the pure shear problem with doubly-periodic boundary conditions and (b) the small scale yielding crack problem with imposed mode I loading.

of the crack tip and symmetry about the crack plane $x_2 = 0$ is assumed. Remote from the crack tip, displacements corresponding to the linear elastic mode I K-field are applied. Crack growth is modelled using a cohesive surface framework, as in Needleman [18]. Dislocation nucleation from the crack tip is not modelled. For computational convenience, dislocation activity is restricted to a process region of dimensions $L_p \times h_p = 15\,\mu\text{m} \times 15\,\mu\text{m}$ (see figure 1b). The finite element mesh, which is the same for all grain sizes, consists of 132×92 rectangular bilinear displacement elements, with a 72×72 element mesh in the process region. A graduated mesh is used with a minimum element size of about $0.05\,\mu\text{m} \times 0.05\,\mu\text{m}$ near the crack tip. Computations are terminated before any dislocations reach the boundary of the process region so that the effect of the process region is to restrict the loading range that can be analysed. The process region consists of uniformly-sized square grains with sizes ranging from $d = 0.2\,\mu\text{m}$ to $5\,\mu\text{m}$. For reference, calculations with only one grain in the process region are also carried out; since the computations are terminated before dislocations reach the boundary of the process region, this corresponds to a single crystal calculation.

Along the cohesive surface, symmetry requires $T_1 = 0$ while the magnitude of T_2 has the universal binding form [19],

$$T_2(\Delta_2) = \sigma_{\text{coh}} \frac{\Delta_2}{\delta_n} \exp\left(1 - \frac{\Delta_2}{\delta_n}\right), \tag{5}$$

where $\Delta_2 = 2u_2(x_1, 0^+)$ is the cohesive opening, σ_{coh} is the cohesive strength and δ_n is a characteristic length. The work of separation is given by $\varphi_n = \exp(1)\sigma_{\text{coh}}\delta_n$ and is related to a reference stress intensity factor K_0 by

$$K_0 = \sqrt{\frac{E\varphi_n}{1 - \nu^2}}. \tag{6}$$

The significance of K_0 is that mode I crack growth in a homogeneous elastic solid with the given cohesive properties takes place at $K_I/K_0 = 1$. In all stationary crack computations, the cohesive properties were taken as $\sigma_{\text{coh}} = 5\,\text{GPa}$ and $\delta_n = 7.5\,\text{nm}$. Choosing such a high value for the cohesive strength gives a K_0 large enough to preclude crack growth for the applied K_I values considered here. All calculations were carried out with a rather high loading rate of $\dot{K}_I = 100\,\text{GPa}\sqrt{\text{m}}\,\text{s}^{-1}$. Although the effect of loading rate is not explored here, it is worth noting that Cleveringa *et al.* [20] found that variations in the loading rate by two orders of magnitude did not change the crack growth behaviour qualitatively, although, of course, a strong tendency was found for increased plastic deformation at lower loading rates.

2.4. *Geometry of polycrystals analysed*

The polycrystals analysed consist of two grain orientations in three arrangements. The two orientations are projections of particular three-dimensional orientations of fcc and bcc crystals that lead to plane strain plastic deformation, as studied by Rice [5]. The fcc orientation has slip systems oriented $\pm 54.7^\circ$ and 0° relative to the x_1-axis. The bcc orientation has slip systems at $\pm 35.3^\circ$ and 90° which corresponds to

a 90° rotation of the fcc orientation. Here, in contrast to Rice [5], the dislocation source strengths are taken to be equal on all slip systems. Thus, the crystals analysed are not fcc and bcc crystals, but are planar crystals with an fcc-like or a bcc-like orientation of slip systems. However, we use the terms fcc crystal and bcc crystal for convenient identification of these two orientations.

The three grain arrangements are: (i) rows of the same grain type, where each row differs in type from the two rows adjacent to it, (ii) columns of the same grain type, where each column differs in type from the two columns adjacent to it, and (iii) an arrangement of alternating grains, analogous to a checker-board, where each grain differs in type from its four adjacent neighbors. In all crack calculations, the process window consists of an odd number of grains. There are six grain arrangements for the polycrystal mode I crack problem, as depicted in figure 2;

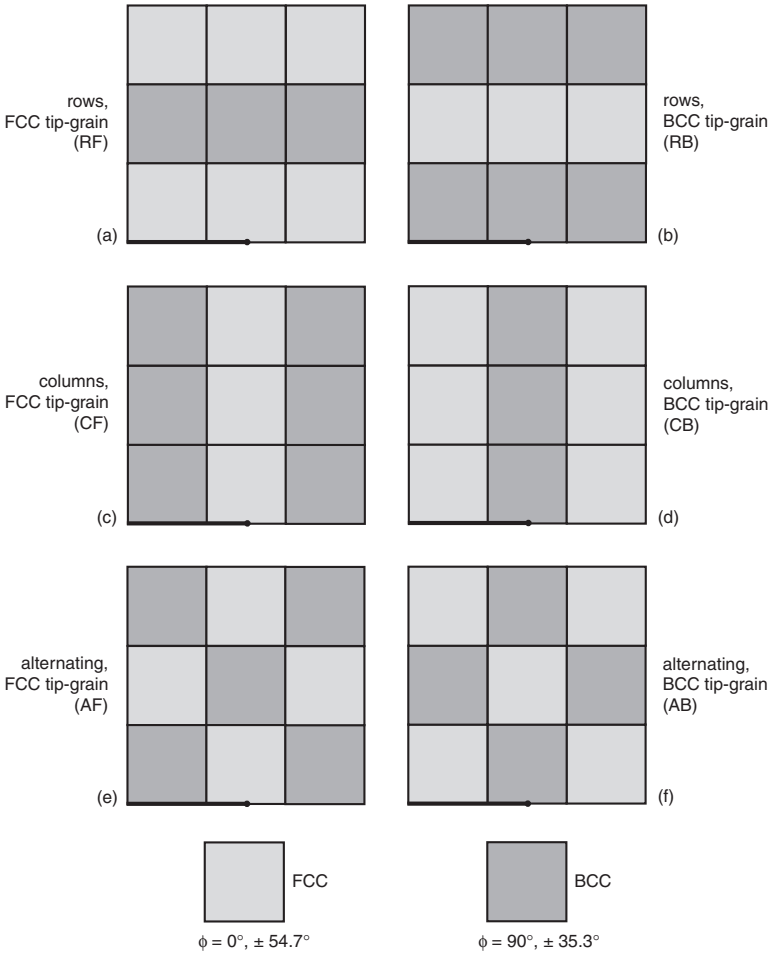

Figure 2. The six polycrystalline grain arrangements used in the mode I crack simulations. The arrangements are illustrated for a 3×3 array of grains with the crack plane indicated by the dark line.

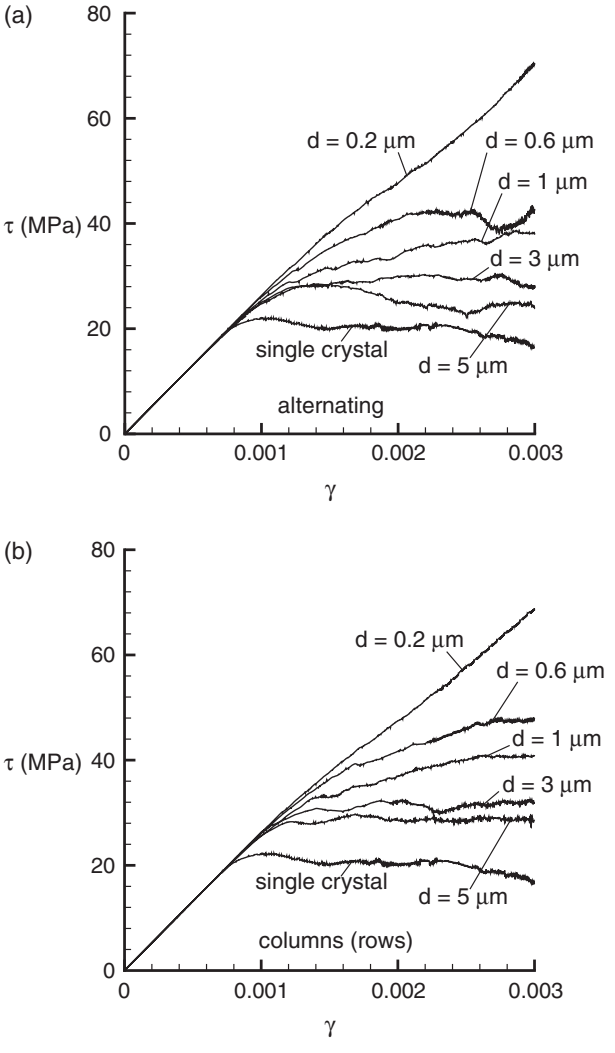

Figure 3. The applied shear stress τ versus shear strain γ response of the polycrystalline and single crystal materials analysed in this study: (a) the alternating (checker-board) grain arrangement (b) the column (or, equivalently, row) grain arrangement (figure 2).

three of these have an fcc grain at the crack tip and three a bcc grain. Subsequently, these arrangements are referred to as RF for the row arrangement with an fcc crack-tip grain (figure 2a) and RB for the row arrangement with a bcc crack-tip grain (figure 2b); CF for the column arrangement with an fcc crack-tip grain (figure 2c) and CB for the column arrangement with a bcc crack-tip grain (figure 2d); AF for the alternating (checker-board) arrangement with an fcc crack-tip grain (figure 2e) and AB for the alternating (checker-board) arrangement with a bcc crack-tip grain (figure 2f). Unless otherwise noted, the crack tip is taken to be at the mid-point of the crack-tip grain.

Only two of the six polycrystal arrangements used in the mode I crack calculations are unique when subjected to doubly-periodic pure-shear boundary conditions: a column (or, equivalently, row) arrangement, and a checker-board arrangement. Thus, only the RF and AF arrangements were employed in the shear calculations. Furthermore, there is no difference between the response of the fcc and bcc single crystals in pure shear since both the crystal geometry and the boundary conditions are invariant under a 90° rotation. For all pure shear calculations, the volume fraction of each of the two grain types is 50% and the number of grains per side of the unit cell is even so that periodicity is maintained.

3. Numerical results

3.1. *Pure shear*

The shear stress, τ, versus shear strain, γ, curves for the polycrystalline materials analysed are plotted in figures 3a and 3b, for the column (or, equivalently, row) and alternating (checker-board) arrangements of fcc and bcc grains. The shear stress versus shear strain responses of the single crystals are also included. Comparison of figures 3a and 3b shows that the grain arrangement has a relatively small influence on the τ versus γ curves, especially for the small grain sizes, and thus the subsequent discussion is relevant for both grain arrangements.

Following an initial linear elastic response (which is uniform since the crystals are elastically isotropic), yield is seen in all cases as a deviation from the elastic response, with the yield strength increasing with decreasing grain size d. The large grained polycrystals have a nearly ideally plastic response. However, the hardening rate increases with decreasing grain size and the small grain-size polycrystals exhibit a very high hardening rate. The shear flow strength, $\bar{\tau}$, defined as the average shear stress between $\gamma = 0.15\%$ and 0.25%, is plotted in figure 4 for both grain arrangements as a function of the grain size d. (Note that $\bar{\tau}$ gives an offset yield strength and for the purposes of the subsequent discussion, we will identify $\bar{\tau}$ with the continuum shear yield strength τ_Y of the material.) For both grain arrangements, $\bar{\tau}$ increases with decreasing d. A Hall–Petch type relation of the form

$$\bar{\tau} - \tau_0 = \beta \left(\frac{d}{d_0} \right)^{-q} \tag{7}$$

is fit to the data in figure 4 where τ_0 is the shear flow strength $\bar{\tau}$ of the single crystal and d_0 is a reference grain size taken to be 1 μm. Equation (7) with $q = 0.415$, $\beta = 15.316$ MPa and $\tau_0 = 20$ MPa fits the data for both grain arrangements very well, which suggests that the shear strength of these polycrystals scales with grain size consistent with a Hall–Petch type relation.

3.2. *Mode I stationary crack*

Since the ($\tilde{}$) fields are given analytically, the finite element mesh needs to resolve the ($\hat{}$) fields, not the total fields. Thus, the element size is taken so as to resolve the ($\hat{}$) field gradients in the vicinity of the crack tip. An estimate of the length scale over

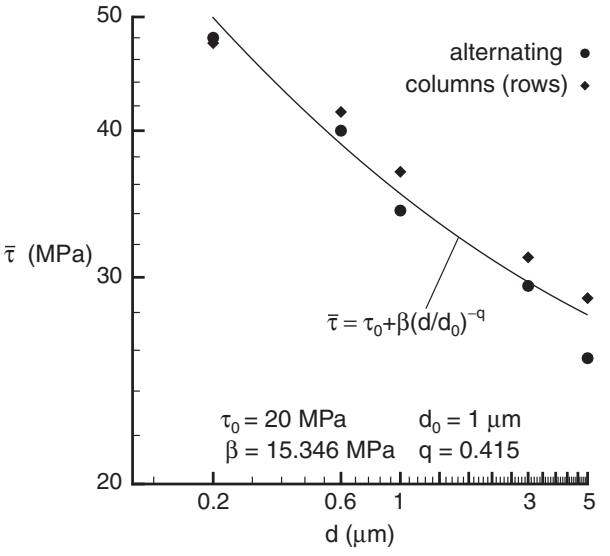

Figure 4. Average shear stress $\bar{\tau}$ between $\gamma = 0.15\%$ and 0.25% for both grain arrangements as a function of grain size d. The Hall–Petch type relation equation (7) is fit to the data.

which gradients occur in the vicinity of a cohesive crack tip is, as discussed by Morrisey and Rice [21], proportional to $(E/\sigma_{\text{coh}})\delta_n \approx 0.1\,\mu\text{m}$. In the stationary crack calculations, the size of the smallest element side is about half this cohesive length. Figures 5a and 5b show contours of the normalized stress $\hat{\sigma}_{22}/\bar{\tau}_{\text{nuc}}$ around the crack tip at $K_I/K_0 = 1.75$ for the fcc single crystal and for the AF polycrystal with grain size $d = 0.6\,\mu\text{m}$, respectively. The ($\hat{}$)-stress field varies little between the single crystal and the polycrystal, is smoothly varying in both cases and is readily resolved by the finite element mesh employed. It is worth noting that while the $\hat{\sigma}_{22}$ fields in both the single and polycrystal cases are very similar, the total σ_{22} fields differ substantially (as seen subsequently in figure 10).

In order to visualize the deformation in the vicinity of the crack tip, we plot the distribution of plastic slip. The calculation of the plastic slip involves averaging the displacement jumps across slip planes. In particular, the values of the displacements are evaluated on a uniform grid of square cells having side lengths approximately $0.2\,\mu\text{m}$. The strain field ϵ_{ij} is then obtained by numerical differentiation. The slip $\gamma^{(\alpha)}$ is defined by

$$\gamma^{(\alpha)} = s_i^{(\alpha)} \epsilon_{ij} m_j^{(\alpha)}, \tag{8}$$

where $s_i^{(\alpha)}$ is the tangent and $m_j^{(\alpha)}$ is the normal to slip system α. The quantity $\gamma^{(\alpha)}$ is not the actual slip on slip system α, as it includes contributions from dislocations gliding on all slip systems; however, it is a convenient quantity for picturing the deformation pattern.

Contours of total slip, $\Gamma = \sum_{\alpha=1}^{3} |\gamma^{(\alpha)}|$, are plotted in figure 6 for the AF grain arrangement (figure 2e) at $K_I/K_0 = 1.75$; while figure 6a pertains to the fcc single

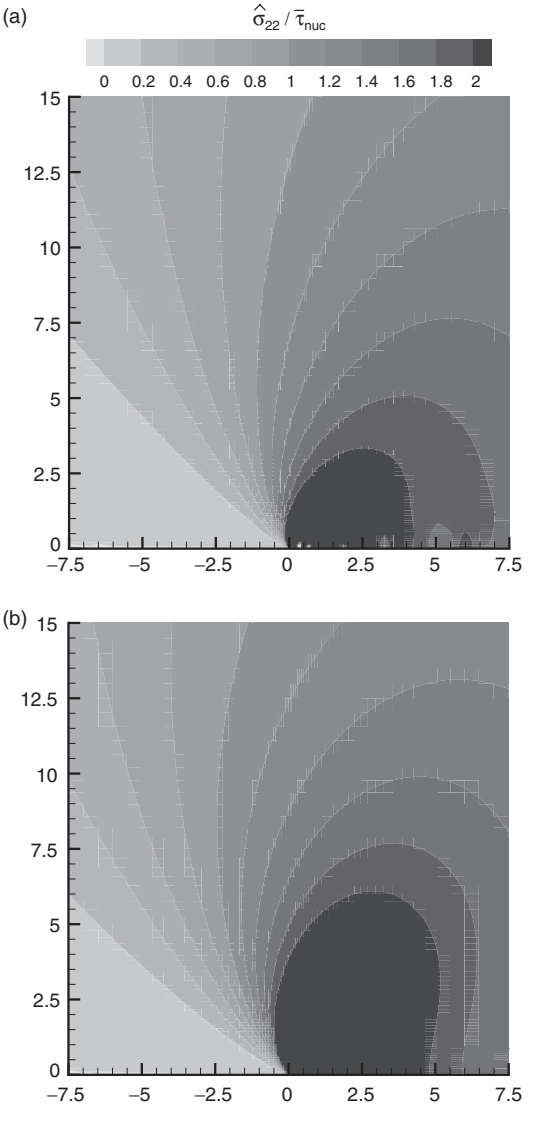

Figure 5. Distributions of the normalized (ˆ) stress, $\hat{\sigma}_{22}/\bar{\tau}_{\text{nuc}}$, around the stationary crack tip at an applied $K_I/K_0 = 1.75$ in (a) the fcc single crystal and (b) the AF grain arrangement (figure 2e) with $d = 0.6\,\mu\text{m}$. (All distances are in μm.)

crystal, figures 6b through 6f show contours of Γ for the $d = 5\,\mu\text{m}$ through $d = 0.2\,\mu\text{m}$ polycrystals in descending order. With decreasing grain size, we observe:

(i) The fcc single crystal deforms in a distinctly anisotropic manner, with slip bands forming on all the three slip systems as seen previously by Van der Giessen *et al*. [17]. On the other hand, with decreasing grain size, slip is seen to be more diffuse with the stress distributions resembling an almost isotropic HRR field for the $d = 0.6\,\mu\text{m}$ and $0.2\,\mu\text{m}$ polycrystals.

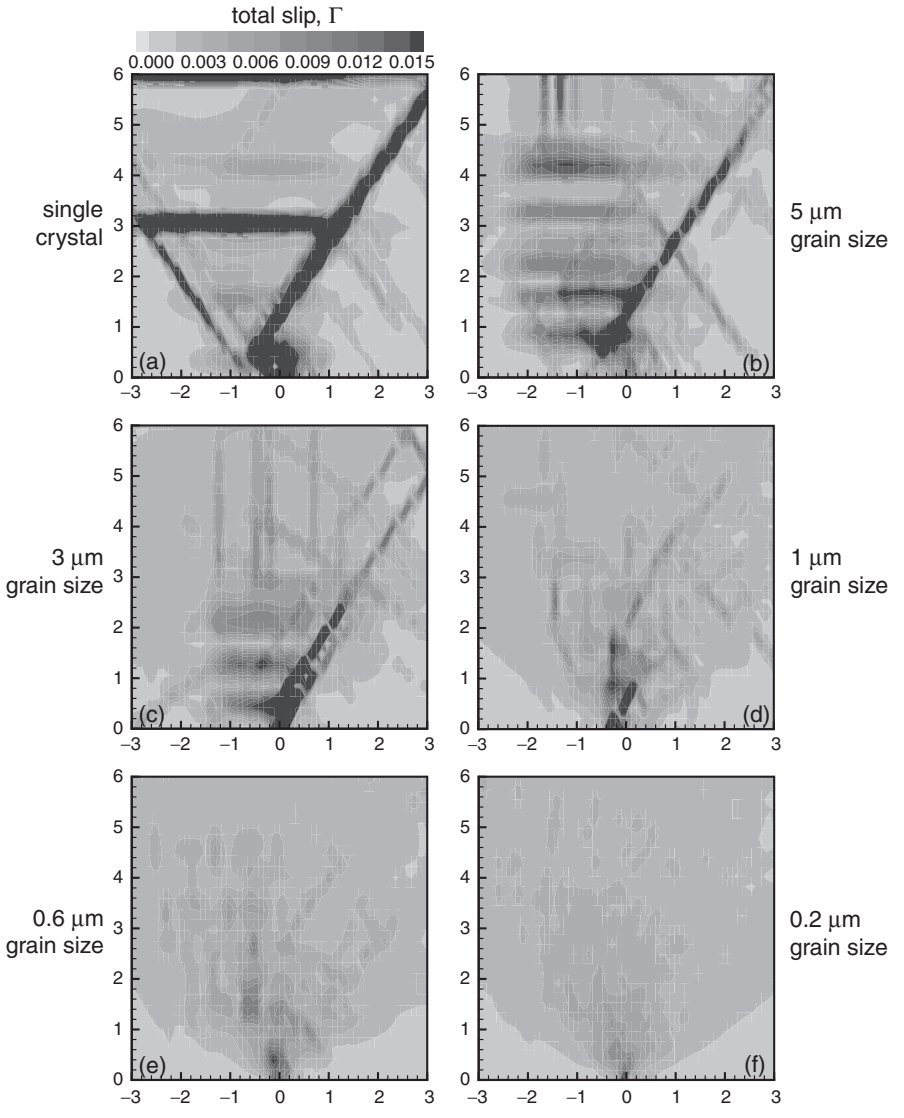

Figure 6. Distributions of total slip Γ around the stationary crack tip of polycrystals with the AF grain arrangement (figure 2e) at an applied $K_I/K_0 = 1.75$: (a) pertains to the fcc single crystal and (b) through (f) are for the $d = 5\,\mu m$ to $d = 0.2\,\mu m$ polycrystals, in descending order. (All distances are in μm.)

(ii) The slip magnitude Γ decreases with decreasing grain size and slip is more confined to the near crack-tip region in the small-grained polycrystals: slip magnitudes $\Gamma \geq 0.015$ occur out to a distance $\approx 0.2\,\mu m$ from the crack tip for the $d = 0.2\,\mu m$ polycrystal while similar levels of Γ extend to a radius of at least 6 μm for the fcc single crystal.

The effect of grain arrangement on the deformation fields around the crack tip is illustrated in figure 7 for the polycrystal with grain size $d = 0.6\,\mu m$. Other than the CB grain arrangement (figure 2d), the contours of Γ around the crack tip at $K_I/K_0 = 1.75$ are remarkably similar with plasticity confined to within a distance $\approx 0.6\,\mu m$ from the crack tip. In the CB grain arrangement case, a slip band on the 90° slip planes extends about three grains above the crack tip to $\approx 1.8\,\mu m$. This is in contrast to the bcc single crystal (figure 8) where the 90° slip band above the crack tip extends to more than $6\,\mu m$. Thus, while the grain boundaries are reasonably successful in blocking slip, some anisotropy of slip can persist when grains are favorably aligned.

In order to investigate the degree of anisotropy of the deformation fields we plot the trajectory in strain-space of the average total strains at $K_I/K_0 = 1.75$. A strain-space plot with ϵ_{12} on the vertical axis and $(\epsilon_{11} - \epsilon_{22})/2$ on the horizontal axis was employed by Shield and Kim [22] to present their experimental measurements of strain around a crack tip. This is analogous to the stress-space employed by Rice [5] to plot the yield surfaces of the fcc and bcc single crystals. First, consider the strain-space plots of the fcc and bcc single crystals in figure 9a where the strains are averaged radially between $r = 0.5\,\mu m$ and $1.5\,\mu m$, and are plotted as a function of the angle θ measured anticlockwise from the crack plane. For the bcc single crystal, two distinct peaks are seen at $\theta \approx 90^\circ$ and 145°, corresponding to the formation of slip bands on the $\phi = 90^\circ$ and -35.3° slip systems. On the other hand, no clear strain peaks are seen for the fcc single crystal even though distinct slip bands are seen in figure 6a. This is because the slip bands do not exactly intersect the crack tip. A more appropriate way of plotting the data for the fcc single crystal is to sample over an annulus centered at $(-0.75, 0.0)\,\mu m$ with inner and outer radii of $1.5\,\mu m$ and $2.5\,\mu m$. This plot, shown as an inset in figure 9a, displays a large peak at $\theta \approx 55^\circ$ corresponding to the slip band on the $\phi = 54.7^\circ$ slip system and a much smaller peak corresponding to the slip band on the $\phi = -54.7^\circ$ slip system. These results for the single crystal slip patterns are consistent with the results in Van der Giessen *et al*. [17]; away from the very near crack-tip region, the discrete dislocation results agree reasonably well with the continuum non-hardening solutions of Drugan [23] and Rice [5] for the fcc and bcc single crystal geometries, respectively.

Next, we consider the $d = 0.6\,\mu m$ polycrystal at $K_I/K_0 = 1.75$. The strain-space plots for all grain arrangements are shown in figure 9b with the strains averaged in an annular region between $r = 0.2\,\mu m$ and $r = 1.2\,\mu m$ (centered at the crack tip). An annulus with an inner radius closer to the crack tip is chosen to ensure that the region over which plastic deformation occurs in the $d = 0.6\,\mu m$ polycrystal is sampled (figure 7e). In contrast to the strain-space plots for the fcc and bcc single crystals, the strain-space plots for the $d = 0.6\,\mu m$ grain size are all nearly identical and approximately circular with no distinct peaks except for the AF grain arrangement (the inset in figure 9b shows a magnified view of the strain-space plot of the AF grain arrangement). The peak at $\theta = 40^\circ$ in the strain-space plot of the AF grain arrangement (figure 2e) is associated with extensive slip on the $\phi = 54.7^\circ$ slip system in the crack-tip grain; the slip in the crack-tip grain dominates the average slip calculated in the annular region between $r = 0.2\,\mu m$ and $r = 1.2\,\mu m$. Also, consistent with the reduction in plastic zone size with decreasing grain size (figure 6), the slip magnitude

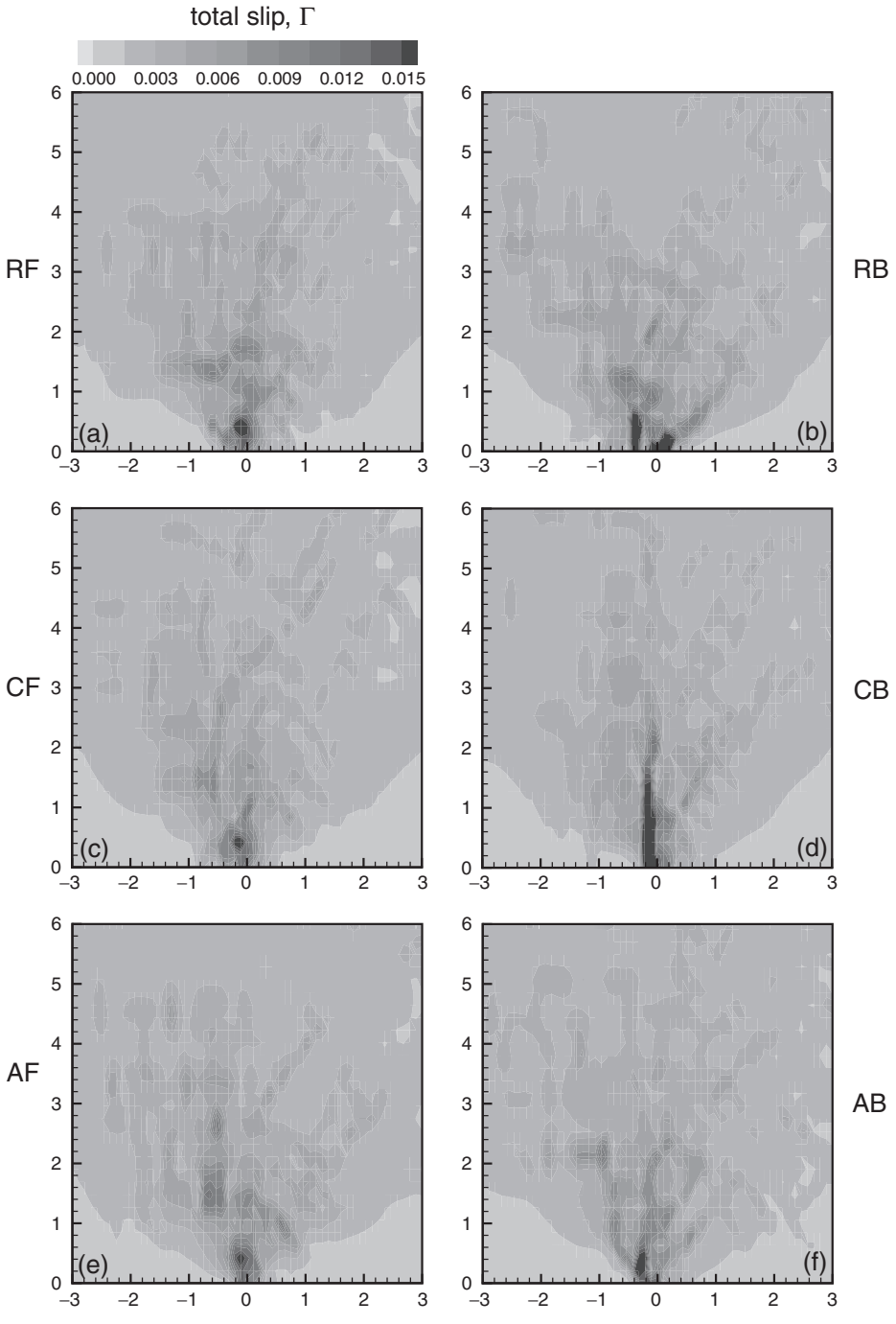

Figure 7. Distributions of total slip Γ around the stationary crack tip of the $d = 0.6\,\mu m$ polycrystalline materials at an applied $K_I/K_0 = 1.75$: (a) through (f) are for the grain arrangements in figures 2a through 2f, respectively. (All distances are in μm.)

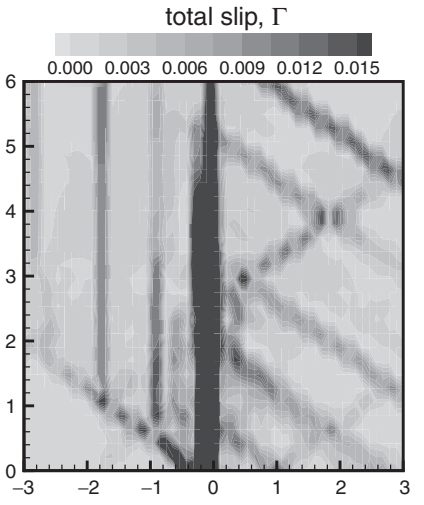

Figure 8. Distribution of total slip Γ around the stationary crack tip in the bcc single crystal at $K_I/K_0 = 1.75$. (All distances are in μm.)

is much smaller for the $d = 0.6\,\mu\text{m}$ polycrystals than for the fcc and bcc single crystals.

The distribution of total opening stress, σ_{22}, is plotted in figures 10a and 10b for the fcc single crystal and the AF polycrystal with $d = 0.6\,\mu\text{m}$ at $K_I/K_0 = 1.75$. Consistent with the strain distributions discussed above, sectors of constant stress are seen to develop around the crack tip in the fcc single crystal in line with the discrete dislocation calculations of Van der Giessen *et al*. [17] and the continuum predictions of Drugan [23]. In contrast, the stress distribution for the $d = 0.6\,\mu\text{m}$ polycrystal is seen to more closely resemble the isotropic HRR predictions. Thus, both the stress and strain fields around the crack tips in our polycrystal analyses indicate that the grain boundaries successfully block the formation of slip bands and tend to diffuse plastic deformation which results in more isotropic distributions of stress and strain. The crack opening profiles (with displacements magnified by a factor of 50) are also included in figure 10. These profiles indicate that for the same applied K_I, substantial blunting occurs in the fcc single crystal, whereas the crack profile is sharper in the $d = 0.6\,\mu\text{m}$ polycrystal.

In order to quantify the effect of grain size on the crack opening displacement, we define an average crack-tip opening displacement, $\bar{\delta}$, as

$$\bar{\delta} = \frac{2}{D}\int_{-D}^{0} u_2(x_1, 0^+)\, dx_1, \tag{9}$$

where $D > 0$ is the length over which the crack-tip opening displacement is averaged. In figure 11a, $\bar{\delta}$ is plotted as a function of the grain size d for the AF grain arrangement (figure 2e) at $K_I/K_0 = 1.75$ for selected values of D in the range $0.5\,\mu\text{m} \le D \le 7.5\,\mu\text{m}$. A small averaging length ($D \le 1.0\,\mu\text{m}$) results in $\bar{\delta}$ being affected by slip steps left by dislocations exiting from the crack plane while this effect is negligible for the larger values of D. In any case, the choice of D only affects the

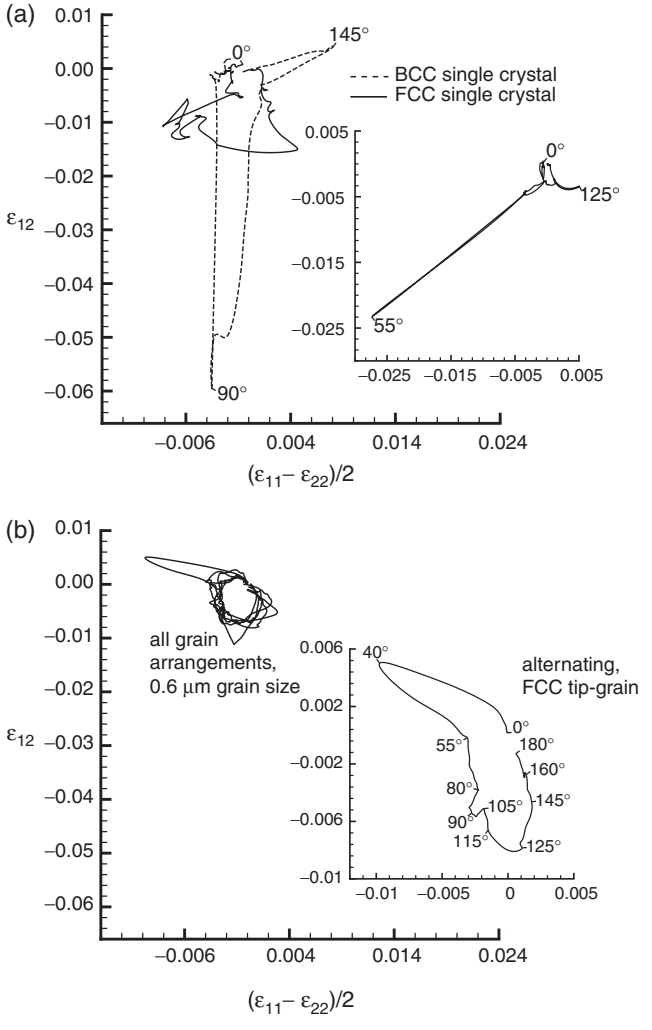

Figure 9. Strain-space plots for the stationary crack at $K_I/K_0 = 1.75$: (a) fcc and bcc single crystals. The inset shows the strain-space plot for the fcc case with the annulus of sampling centered at $(-0.75, 0.0)\,\mu$m. (b) All six grain arrangements with grain size $d = 0.6\,\mu$m. The inset shows a magnified version of the strain-space plot for the AF grain arrangement (figure 2e).

magnitude of $\bar{\delta}$ and not the scaling of $\bar{\delta}$ with grain size d; we use $D = 7.5\,\mu$m here. The variation of the crack-tip opening displacement $\bar{\delta}$ with K_I/K_0 is plotted in figure 11b for the polycrystals with the AF grain arrangement and for the fcc single crystal.

Since there is no material length parameter in isotropic hardening plasticity, under small scale yielding conditions, quantities with the dimension of length, such as the plastic zone size and the crack-tip opening displacement, scale with K_I^2/τ_Y, where τ_Y is the continuum shear yield strength of the material. In figure 11b the scaling with K_I^2 holds approximately.

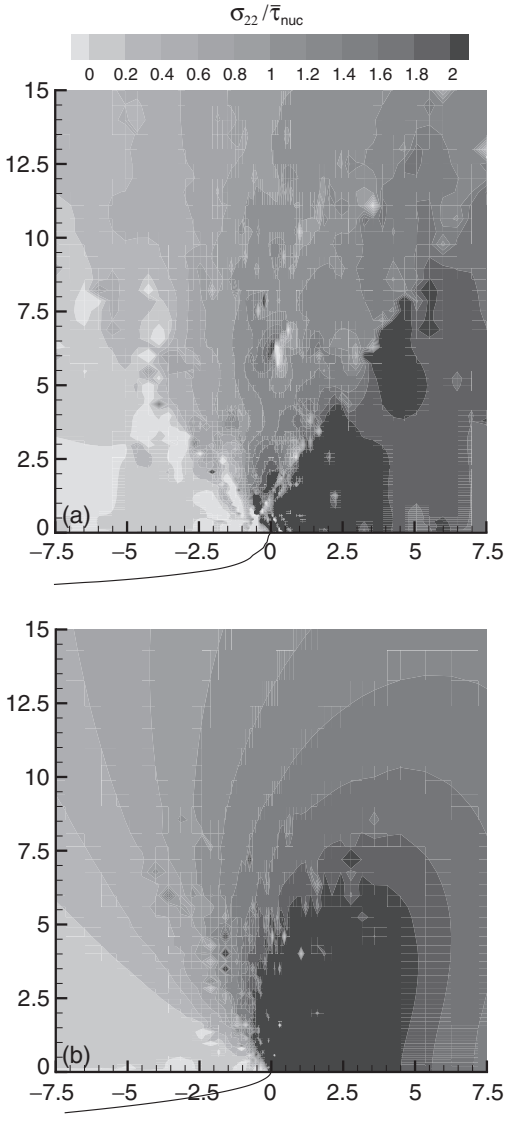

Figure 10. Distributions of normalized stress, $\sigma_{22}/\bar{\tau}_{\text{nuc}}$, around the stationary crack tip at $K_I/K_0 = 1.75$: (a) the fcc single crystal (b) the AF grain arrangement (figure 2e) with $d = 0.6\,\mu\text{m}$. The crack-tip profile with displacements magnified by a factor of 50 is included in both cases. (All distances are in μm.)

The effect of grain size on $\bar{\delta}$ is shown in figure 12 for all the polycrystal grain arrangements at $K_I/K_0 = 1.75$. Figure 12 indicates that $\bar{\delta}$ is not sensitive to the grain arrangement, with $\bar{\delta}$ increasing with increasing d. Motivated by the continuum relation $\bar{\delta} \propto 1/\tau_Y$, with τ_Y identified with $\bar{\tau}$ given by equation (7), a relation of the form

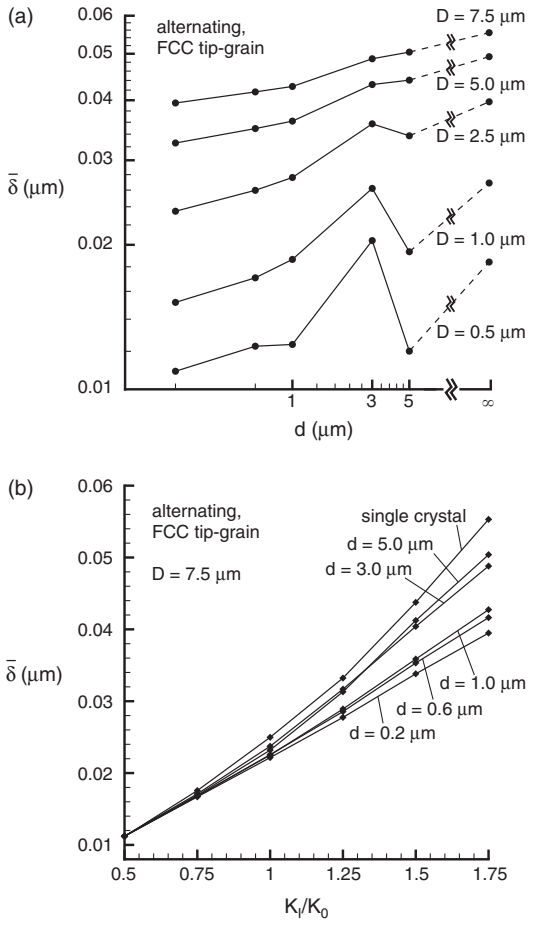

Figure 11. (a) Variation of the crack-tip opening displacement, $\bar{\delta}$, averaged over a length D behind the crack tip, with grain size d. Results are shown for selected values of the averaging length D. (b) $\bar{\delta}$ with the choice $D = 7.5\,\mu m$ as a function of the applied K_I for all grain sizes of the AF grain arrangement (figure 2e).

$$\bar{\delta} = \frac{\delta_0}{1 + \eta(d/d_0)^{-p}} \tag{10}$$

is fit to the data, where δ_0 is the value of $\bar{\delta}$ for the single crystal, d_0 is a reference grain size (taken to be $1\,\mu m$) and η and p are constants that are determined from a least-squares fit. In equation (10), $\bar{\delta}$ approaches the single crystal value as d increases, but as $d \to 0$, $\bar{\delta} \to 0$ rather than approaching the elastic value. The fit included in figure 12 uses the values $\eta = 0.226$ and $p = 0.387$ with $\delta_0 = 0.055\,\mu m$, the average of the fcc and bcc single crystal crack-tip opening displacements at $K_I/K_0 = 1.75$. We observe that $p \approx q$, the exponent in the Hall–Petch type relation, equation (7), that relates the polycrystal shear yield strength to grain size, indicating that,

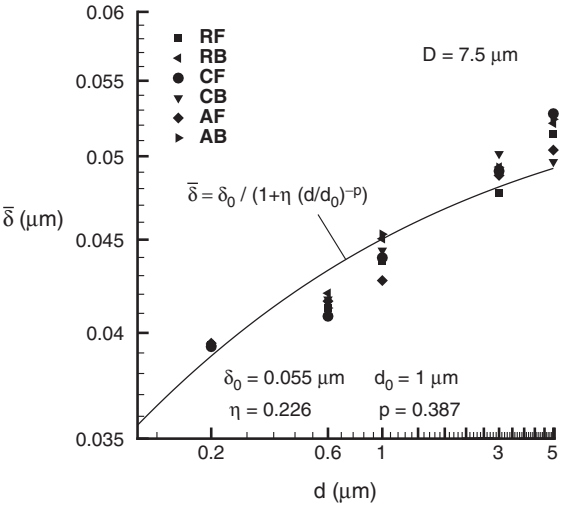

Figure 12. The crack-tip opening displacement $\bar{\delta}$ ($D = 7.5\,\mu\text{m}$) at an applied $K_I/K_0 = 1.75$ for all six grain arrangements as a function of the grain size d. Equation (10) is fit to the data and plotted as a solid line in the figure.

with $\bar{\tau}$ identified with the continuum plasticity shear yield strength τ_Y, $\bar{\delta} \propto 1/\tau_Y$ is consistent with the continuum isotropic plasticity prediction.

Discrete dislocation results for the crack opening stress ahead of the crack, $\sigma_{22}(x_1 > 0, x_2 = 0)$, are plotted in figure 13 for three selected grain sizes $d \leq 3\,\mu\text{m}$ as a function of the distance r from the crack tip for the AF polycrystals at an applied $K_I/K_0 = 1.75$. The plot shows the existence of three regimes. For all grain sizes, $\sigma_{22} \propto 1/\sqrt{r}$ for $r > 5\,\mu\text{m}$ as per the applied elastic K-field. Although fluctuations in σ_{22} occur due to the stress concentrations associated with individual dislocations very near the crack plane, the scaling in the range $0.2\,\mu\text{m}$ to $2\,\mu\text{m}$ is investigated by fitting σ_{22} to an HRR-type relation

$$\frac{\sigma_{22}}{\bar{\tau}_{\text{nuc}}} = \kappa\left(\frac{r_0}{r}\right)^{(1/(s+1))}, \tag{11}$$

where κ is a dimensionless fitting parameter, r_0 is a reference length taken to be $1.0\,\mu\text{m}$, and s is the strain hardening exponent in a shear stress τ versus shear strain γ relation of the form $\gamma \propto \tau^s$. Least-squares fits to the discrete dislocation results in the range $0.2\,\mu\text{m} \leq r \leq 2.0\,\mu\text{m}$ are included in figure 13a and the associated values of κ and s are listed in table 1. The value of s increases with increasing grain size d: $s \to \infty$ for $d = 3\,\mu\text{m}$ as this polycrystal exhibits a nearly ideally plastic τ versus γ response, while for $d = 0.2\,\mu\text{m}$, $s \approx 1$ as the τ versus γ relation of this polycrystal is nearly elastic (figure 3a).

The values of s obtained from the crack-tip stress fit, equation (11), are consistent with the strain hardening behaviours in pure shear. To show this, we fit a piecewise τ versus γ relation of the form

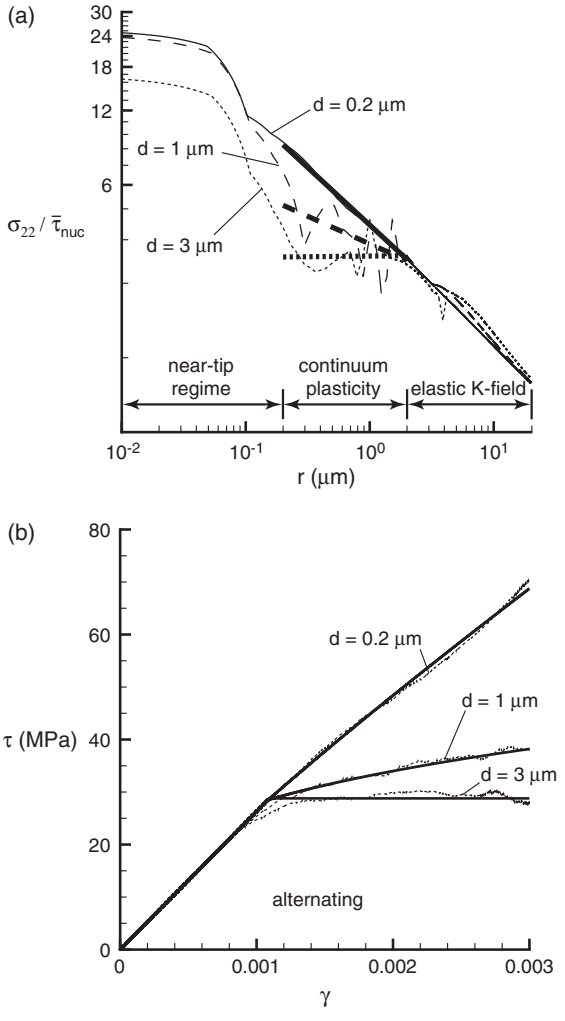

Figure 13. (a) Normalized crack opening stress, $\sigma_{22}/\bar{\tau}_{nuc}$, on the crack plane ahead of the stationary crack tip at an applied $K_I/K_0 = 1.75$ for the AF grain arrangement (figure 2e). Results are plotted for three selected grain sizes d and fits to equation (11) for the continuum plasticity regime are also included (thick lines). (b) The applied shear stress versus shear strain curves for the polycrystals in (a) (figure 3a). Piecewise power-law fits, equation (12), employing the exponents s from table 1 are shown by the thick lines.

Table 1. The values of κ and s obtained by a least-squares fit of equation (11) to the discrete dislocation data in figure 13 in the range $0.2\,\mu m \leq r \leq 2.0\,\mu m$.

d (μm)	κ	s
0.2	4.131	1.155
1.0	3.464	3.476
3.0	3.091	$\rightarrow \infty$

$$\frac{\gamma}{\gamma_Y} = \begin{cases} \dfrac{\tau}{\tau_Y} & \text{if } \tau \le \tau_Y\,; \\ \left(\dfrac{\tau}{\tau_Y}\right)^s & \text{otherwise}\,, \end{cases} \tag{12}$$

where $(\tau_Y/\gamma_Y) = (E/2(1+\nu))$, to the pure shear response for the $d = 3\,\mu\text{m}$, $1\,\mu\text{m}$ and $0.2\,\mu\text{m}$ polycrystals from figure 3a. The fits using the values of s from table 1 are shown in figure 13b and agree very well with the corresponding shear stress versus shear strain curves given by the discrete dislocation analyses. Thus, in the $0.2\,\mu\text{m} \le r \le 2.0\,\mu\text{m}$ regime, the discrete dislocation results are consistent with HRR predictions.

In the near crack-tip regime, ($0\,\mu\text{m} \le r \le 0.2\,\mu\text{m}$), σ_{22} deviates considerably from the HRR predictions, being dominated by the stress concentration associated with the near tip dislocation structure and limited by the cohesive strength. In fact, σ_{22} reaches a plateau very near the crack tip ($0 \le r \le 0.1\,\mu\text{m}$) with $\sigma_{22}/\bar{\tau}_{\text{nuc}} \approx 25$ for the $d = 1\,\mu\text{m}$ and $0.2\,\mu\text{m}$ polycrystals and $\sigma_{22}/\bar{\tau}_{\text{nuc}} \approx 16$ for the $d = 3\,\mu\text{m}$ polycrystal. The crack opening stresses are thus higher for the smaller grained polycrystals and are a factor of 4 to 7 greater than the non-hardening continuum plasticity theory predictions. For example, the analysis of Rice [5] gives $\sigma_{22} = 4\sqrt{2}\,\tau_{\text{crss}}$ for the fcc and bcc single crystals, where τ_{crss} is the critical resolved shear stress of a slip system while the Prandtl slip line field gives $\sigma_{22} = (2+\pi)\,\tau_Y$ in an isotropic non-hardening solid [24].

3.3. *Mode I crack growth*

To analyse crack growth, the cohesive properties are taken as $\sigma_{\text{coh}} = 0.5\,\text{GPa}$ and $\delta_n = 0.75\,\text{nm}$ giving a work of separation $\varphi_n \approx 1.0\,\text{J m}^{-2}$ which is representative of many crystalline metals. The initial location of the crack tip is taken to be $(d/2 - 0.3, 0)\,\mu\text{m}$ for the $d \ge 0.6\,\mu\text{m}$ cases, while in the $d = 0.2\,\mu\text{m}$ case the crack tip is located at $(0,0)\,\mu\text{m}$ in order to ensure that the crack crosses at least one grain boundary in the computations. The computed curves of applied stress intensity factor, K_I, versus crack extension, Δa, are shown in figures 14a and 14b for the AF (figure 2e) and AB (figure 2f) grain arrangements, respectively. The fcc and bcc single crystal crack growth resistance curves are also included in figure 14. The location of the current crack tip is defined as the furthest point from the initial crack tip where Δ_n exceeds $4\delta_n$. In all cases, crack growth initiates at $K_I/K_0 \approx 1.0$. Subsequently, there is a sharp increase in the crack growth resistance of the $d > 1\,\mu\text{m}$ polycrystals with crack growth occurring in spurts similar to the single crystals results of Cleveringa *et al.* [7]. In these cases, fracture did not occur for the range of values of applied K_I considered here. In contrast, fracture occurred for $d \le 0.6\,\mu\text{m}$ and $d \le 1\,\mu\text{m}$ polycrystals with an fcc and bcc crack-tip grain, respectively (fracture is identified with onset of unstable crack growth and is denoted by an X in figure 14). The fracture toughness K_{IC}, defined as the value of K_I at which unstable crack growth occurs, decreases with decreasing d with $K_{\text{IC}} \approx K_0$ for the $d = 0.2\,\mu\text{m}$ polycrystals.

The crack growth behaviours seen in these discrete dislocation calculations are a consequence of the dual role that dislocations play in the fracture process.

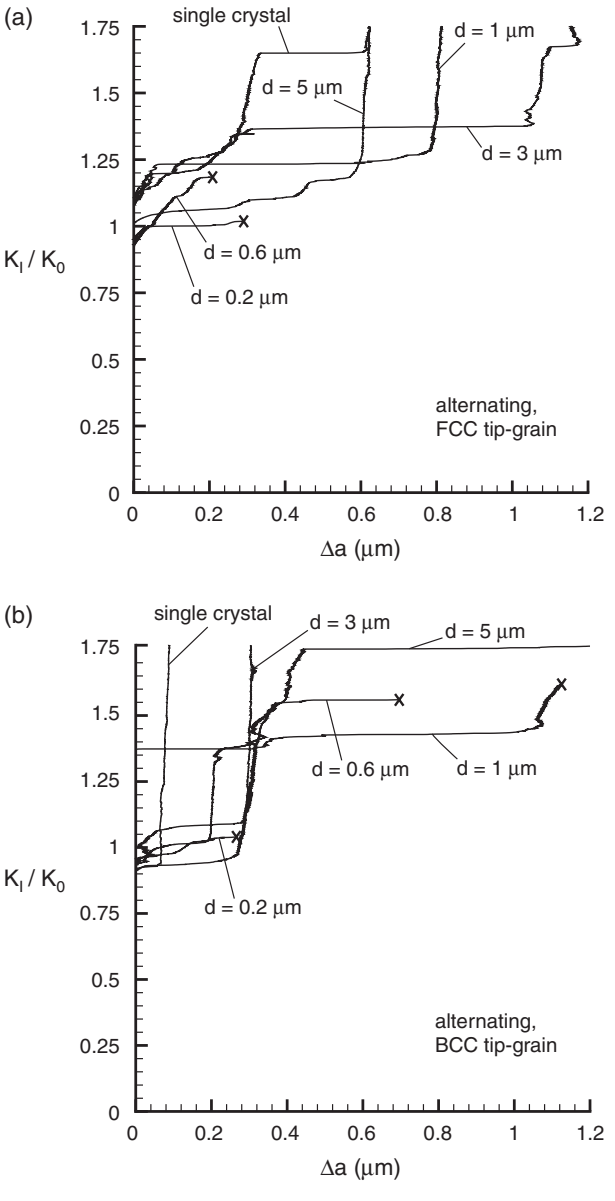

Figure 14. Applied K_I versus crack extension, Δa, for (a) the AF grain arrangement (figure 2e) and (b) the AB grain arrangement (figure 2f). The fcc and bcc single crystal crack growth resistance curves are included in (a) and (b), respectively. An **X** denotes the onset of unstable crack growth.

Although plastic flow due to the motion of dislocations increases the resistance to crack growth, the local stress concentration associated with the discrete dislocation structure near the crack tip promotes crack propagation. As the grain size decreases, the mobility of the dislocations is inhibited by the impenetrable grain

boundaries. Thus, dislocations form clusters around the crack tip, increasing stress levels (figure 13) and promoting crack growth. On the other hand, for large-grained polycrystals and single crystals, dislocations freely glide away from the crack-tip region, thus increasing plastic dissipation and the crack growth resistance.

4. Discussion

As described in Balint *et al*. [16], grain boundaries prevent the formation of easy slip paths across the material. This results in (i) an increase in the yield strength and hardening rate with decreasing grain size d, (ii) a smearing-out of plasticity around the crack tip with the polycrystal crack-tip fields reasonably insensitive to the grain arrangements and resembling isotropic continuum plasticity fields, (iii) reduced plastic zone sizes with decreasing d and (iv) an inverse scaling of the crack-tip opening displacement $\bar{\delta}$ with the shear yield strength τ_Y, which in turn implies a scaling of $\bar{\delta}$ with d. These conclusions apply to materials with the dislocation source density $\rho_{\text{nuc}} = 20\,\mu\text{m}^{-2}$, which is higher than dislocation densities corresponding to Frank networks in well-annealed crystals but is considered representative for crystals that have undergone small amounts of cold-working [12]. For a given grain size, increasing the source density could promote the formation of slip bands that span many grains (as seen by Balint *et al*. [16] for polycrystals subject to pure shear) and thus lead to crack tip fields more like those predicted by single crystal continuum slip plasticity theory.

The discrete dislocation simulations reveal that the fracture toughness K_{IC} of polycrystalline materials decreases with decreasing d: as the grain size decreases, the dislocations form clusters around the crack tip increasing the crack opening stresses and promoting crack growth. There are a number of simplifications in our analyses (in addition to confining attention to planar model crystals) including: (i) restricting the analysis to straight-ahead trans-granular fracture, (ii) excluding transmission through and nucleation from grain boundaries, (iii) neglecting effects of grain boundary particles such as carbides in mild steel and (iv) only considering small amounts of crack growth with the crack typically crossing only one grain boundary in the simulations reported here. In spite of these restrictions, the discrete dislocation results are consistent with the molecular dynamics simulations of Noronha and Farkas [25] on nanocrystalline materials which revealed that blocking of dislocations by obstacles induces brittle behaviour. Such behaviour is also in-line with the fracture model of Ritchie *et al*. [26] which postulates that the macroscopic fracture toughness K_{IC} relates to the attainment of the cleavage stress σ_f over a microstructure-related characteristic length l_0. With this assumption it follows from the HRR fields that

$$K_{\text{IC}} \propto \left[\frac{\sigma_f^{(1+1/s)/2}}{\tau_Y^{(1-1/s)/2}}\right] l_0^{1/2}. \tag{13}$$

For low carbon steels with ferrite–pearlite microstructures, Ritchie *et al*. [26] found that $l_0 \approx 2d$ implying that the fracture toughness increases with increasing grain

size d. Many subsequent experimental investigations (e.g. Curry and Knott [27]) however have not found a consistent scaling of K_{IC} with d. This is primarily thought to be related to the fact that in most metals, the cleavage strength σ_f is itself grain size dependent. For example, Cottrell [28] postulated that micro-cracks form within grains at intersecting slip planes by means of dislocation interaction. Treating these micro-cracks as Griffith cracks of the order of the grain size, it follows that $\sigma_f \propto d^{-1/2}$. In the present study, the local fracture criterion (input into the calculation via the cohesive relation) was independent of the grain size and thus did not include any effects like those postulated by Cottrell [28]. A scaling of K_{IC} with d was not identified from the limited number of crack growth computations carried out here.

In the discrete dislocation simulations presented here, the yield strength and strain hardening rates of the polycrystals emerge from the boundary value problem solutions and are thus themselves a function of d. In fact, the yield strengths follow a Hall–Petch type relation with $\bar{\tau} \propto d^{-0.41}$ (recall that $\bar{\tau}$ is an offset yield strength that we identify with the continuum shear yield strength τ_Y of the material). Thus, the decrease in fracture toughness with decreasing grain size may also be viewed as a decrease in K_{IC} with increasing flow strength, consistent with a wide body of experimental evidence (see, for example, the experimental data in Birkle *et al.* [29] for the effect of yield strength on the fracture toughness of Ni–Cr–Mo steels).

5. Conclusions

We have carried out mode I small-scale yielding analyses of planar polycrystals consisting of various arrangements of planar fcc and bcc-like grains with grain sizes varying from 0.2 μm to 5 μm. The polycrystals are initially dislocation free with dislocation nucleation occurring from Frank–Read sources of a specified density randomly distributed in each grain. There is no special dislocation nucleation from the crack tip.

- Pure shear calculations of the grain arrangements considered give rise to a flow strength that varies with the grain size d as $d^{-0.41}$.
- Grain boundaries blocking slip tend to diffuse deformation which, for a stationary crack, leads to the stress and deformation distribution approaching that of an isotropic plastic solid as the grain size decreases.
  - In the regime $0.2\,\mu m \leq r \leq 2.0\,\mu m$ around the crack tip, the discrete dislocation simulations are consistent with the HRR predictions.
  - Closer to the crack tip, for $r < 0.2\,\mu m$, the discrete dislocation results for a cohesive crack give opening stresses that greatly exceed those predicted by continuum plasticity theory.
- The crack-tip opening displacement varies with grain size as $[1 + \eta(d/d_0)^{-0.39}]^{-1}$. It is (approximately) proportional to K_I^2/τ_Y, which is the expected scaling for small scale yielding of an isotropic plastic solid.
- The crack growth resistance decreases with decreasing grain size.

Acknowledgements

DSB and VSD acknowledge support from the Engineering and Physical Sciences Research Council, UK (EPSRC grant no. GR/S08107/01). AN is pleased to acknowledge support from the General Motors Cooperative Research Laboratory at Brown University.

References

[1] G.R. Irwin, in *Encyclopedia of Physics. Vol. VI. Elasticity and Plasticity*, edited by S. Flügge (Springer-Verlag, Berlin, 1958).
[2] V. Tvergaard and J.W. Hutchinson, J. Mech. Phys. Solids **40** 1377 (1992).
[3] J.W. Hutchinson, J. Mech. Phys. Solids **16** 13 (1968).
[4] J.R. Rice and G. Rosengren, J. Mech. Phys. Solids **16** 1 (1968).
[5] J.R. Rice, Mech. Mater. **6** 317 (1987).
[6] M. Saeedvafa and J.R. Rice, J. Mech. Phys. Solids **37** 673 (1989).
[7] H.H.M. Cleveringa, E. Van der Giessen and A. Needleman, J. Mech. Phys. Solids **48** 1133 (2000).
[8] K.S. Kumar, H. Van Swygenhoven and S. Suresh, Acta Mater. **51** 5743 (2003).
[9] A.H. Chokshi, A. Rosen, J. Karch, *et al*., Scripta Mater. **23** 1679 (1989).
[10] H. Van Swygenhoven, M. Spaczer and A. Caro, Acta Mater. **47** 3117 (1999).
[11] E. Van der Giessen and A. Needleman, Model. Simul. Mater. Sci. Engng **3** 689 (1995).
[12] J. Friedel, *Dislocations* (Addison-Wesley, Reading, MA, 1964).
[13] J.P. Hirth and J. Lothe, *Theory of Dislocations* (McGraw-Hill, New York, 1968).
[14] F.R.N. Nabarro, *Theory of Crystal Dislocations* (Oxford University Press, Oxford, 1967).
[15] L.B. Freund, Adv. Appl. Mech. **30** 1 (1994).
[16] D.S. Balint, V.S. Deshpande, E. Needleman, *et al*., Mater. Sci. Engng A to be published (2005).
[17] E. Van der Giessen, V.S. Deshpande, H.H.M. Cleveringa, *et al*., J. Mech. Phys. Solids **49** 2133 (2001).
[18] A. Needleman, J. Mech. Phys. Solids **38** 289 (1990).
[19] J.H. Rose, J. Ferrante and J. Smith, Phys. Rev. Lett. **47** 675 (1981).
[20] H.H.M. Cleveringa, E. Van der Giessen and A. Needleman, Mater. Sci. Engng A **317** 37 (2001).
[21] J.W. Morrissey and J.R. Rice, J. Mech. Phys. Solids **46** 467 (1998).
[22] T.W. Shield and K.S. Kim, J. Mech. Phys. Solids **42** 845 (1994).
[23] W.J. Drugan, J. Mech. Phys. Solids **9** 2155 (2001).
[24] J.R. Rice, ASTM Spec. Tech. Publ. **415** 247 (1967).
[25] S.J. Noronha and D. Farkas, Mater. Sci. Engng A **365** 156 (2004).
[26] R.O. Ritchie, J.F. Knott and J.R. Rice, J. Mech. Phys. Solids **21** 395 (1973).
[27] D.A. Curry and J.F. Knott, Metal Sci. **13** 341 (1979).
[28] A.H. Cottrell, Theory of brittle fracture in steel and similar metals. Trans. ASME **212** 192 (1958).
[29] A.J. Birkle, R.P. Wei and G.E. Pellissier, Trans. ASM Quarterly **59** 981 (1966).